

High Resolution least-squares wave equation AVA imaging: Feasibility study with a data set from the Western Canadian Sedimentary Basin

Juefu Wang^{*}, University of Alberta, Henning Kuehl, Shell Canada, and Mauricio D. Sacchi, University of Alberta

Summary

This paper presents a regularized least-squares pre-stack 3-D wave equation Amplitude versus Angle (AVA) migration algorithm and explores the feasibility of this class of methods to process field data. We pose seismic imaging as a linear inverse problem that incorporates weighting matrices in model and data space. The goal is to remove additive noise and artifacts that arise from data acquisition, operator mismatch and additive coherent and incoherent noise. We solve the inverse problem with the conjugate gradients method and, in addition, we accelerate the convergence of the CG scheme by a preconditioning strategy.

We have applied the regularized least-squares migration (RLSM) algorithm to a 3-D data set from the Western Canadian Sedimentary Basin. The inversion significantly improves the quality of the common image gathers.

The accuracy of our algorithm is confirmed by a detailed comparison of inverted and synthetic CIGs.

We also observe an substantial enhancement of vertical resolution as a consequence of improving the coherence of the inverted common image gathers and an implicit deconvolution that is embedded in the method.

Introduction

AVA/AVO analysis has been widely used in the industry for oil and gas exploration. High quality AVA estimates are fundamental at the time of estimating hydrocarbon indicators and accessing drilling targets. This has led to important efforts in producing true amplitude angle domain image gathers by prestack migration (see for instance, Xu et al., 1998). Migrated CIGs are quite often contaminated by acquisition-induced artifacts. These artifacts can be attenuated by regularized least-squares wave equation migration (Kuehl and Sacchi, 2003; Wang, Kuehl and Sacchi, 2003).

The major impediment to a practical application of 3-D least-squares migration is computational cost. Each CG iteration involves one full migration/de-migration sequence. In general, *practical* convergence of the conjugate gradients scheme is achieved after 10-20 iterations. The later makes least-squares wave equation migration methods impractical for large 3-D data sets. The problem, however, can be alleviated by using pre-conditioning schemes (Prucha and Biondi, 2001). A remaining question is how to access the fidelity of least squares wave equation migration methods at the time of retrieving AVA gathers from field data, in particular, this is a problem of

concern when imaging 3-D land data with a high degree of spatial incompleteness. The latter could hamper the ability to utilize sophisticated imaging algorithms. Amplitude fidelity studies on synthetic data are provided in Kuehl and Sacchi (2003), but, to our knowledge, the problem has not been studied in detail with 3-D field data.

Regularized least-squares AVA migration

We consider the seismic data as the result of a linear transformation on a model \mathbf{m}

$$\mathbf{d} = \mathbf{L}\mathbf{m} + \mathbf{n} \quad (1)$$

where \mathbf{d} denotes pre-processed seismic data, \mathbf{L} is the forward operator propagator (Kuehl and Sacchi, 2003; Wang et al., 2003), \mathbf{m} indicates the common image gather parametrized in terms of the ray parameter p , and \mathbf{n} denotes additive noise. Conventional migration entails applying \mathbf{L}' , the adjoint of \mathbf{L} , to the observed data. Sava et al. (2002) proposed a Jacobian-corrected migration method to estimate true amplitude common image gathers. In general, this correction does not guarantee proper amplitude fidelity in situations where the image is corrupted by artifacts that are introduced by inadequate spatial sampling. These artifacts can be attenuated, however, by constraining the solution to exhibit certain degree of smoothness along the ray parameter axis. In this case, we adopt the following cost function to retrieve a migrated image that *fits* the observations and, in addition, exhibits smoothness or continuity along the ray parameter axis:

$$F(\mathbf{m}) = \|\mathbf{W}(\mathbf{d} - \mathbf{L}\mathbf{m})\|^2 + \lambda^2 \|\mathbf{D}_{1hx}\mathbf{m}\|^2 \quad (2)$$

where \mathbf{W} is a diagonal weighting matrix used to decrease the influence of missing observations in the migrated image. The regularization operator \mathbf{D}_{1hx} is a first order derivative operator along the in-line ray parameter-offset direction. Least-squares migration seeks a model \mathbf{m} by minimizing the sum of the two norms. The trade-off parameter λ determines the amount of smoothness. We minimize the objective function using a conjugate gradients algorithm.

The computational cost of the method can be decreased by a preconditioned implementation of the CG algorithm. Pre-conditioning strategies for semi-iterative solvers have been thoroughly studied by the applied mathematics

High resolution 3-D AVA Imaging

community (see for instance, Saad, Y., 1991). Pre-conditioning has also been used in the context of interpolation (Fomel and Claerbout, 2003), Radon processing (Trad et al., 2003) and least-squares migration (Prucha and Biondi, 2002).

Equation (2) can be transformed to its standard form after the following change of variable

$$\mathbf{z} = \mathbf{D}\mathbf{m} \quad (3)$$

The substitution of \mathbf{m} in equation (2) leads to

$$\begin{aligned} F(\mathbf{z}) &= \|\mathbf{W}(\mathbf{d} - \mathbf{L}\mathbf{P}\mathbf{z})\|^2 + \lambda^2 \|\mathbf{z}\|^2 \\ F(\mathbf{z}) &= \|\mathbf{W}(\mathbf{d} - \tilde{\mathbf{L}}\mathbf{z})\|^2 + \lambda^2 \|\mathbf{z}\|^2 \end{aligned} \quad (4)$$

where \mathbf{P} , in theory, is the inverse of \mathbf{D} . It is clear that rather than inverting \mathbf{D} we will replace \mathbf{P} by an operator with features similar to those of the inverse of \mathbf{D} . If \mathbf{D} is a discrete derivative operator (a high-pass operator), then, \mathbf{P} must be a low-pass operator. This rationale is used to choose \mathbf{P} as a low-pass convolutional operator. In our implementation, to apply \mathbf{P} is equivalent to apply 1-D convolution along the p -axis.

Finally, we describe the migration/de-migration algorithm utilized by our inversion scheme. For computational tractability we have chosen double square root propagators for common-azimuth data (Biondi and Palacharlas, 1996) in combination with a split-step correction for lateral velocity variations. The mapping from local wavefields to angle gathers is done via a frequency offset-wavenumber implementation of the Radon transform as described in Prucha et. al (1999).

Field data example

We compared the performance of migration, RLSM and preconditioned RLSM using a field data set from the Erskine area (Southern Alberta, Canada). The data volume is a typical 3-D survey from the Western Canadian Basin. The binned data consist of 157 in-lines and 40 cross-lines. The maximum absolute offset in the data is 3000 meters. The uneven distributions of offsets makes it difficult for wave equation migration methods to produce accurate results. In our approach, missing observations are penalized and therefore, their influence on the final image is attenuated.

In all our tests we have computed common image gathers with an offset ray parameter axis in the range 0-800 $\mu\text{s}/\text{m}$, with a ray parameter interval of 6.25 $\mu\text{s}/\text{m}$. Figure 1 shows the calculated CIGs for the midpoint at in-line #71, cross-line #10. The maximum ray parameter shown is 500 $\mu\text{s}/\text{m}$. Figure 1A portrays the migrated image (equivalent to 1 iteration of the least-squares inversion). Artifacts along the ray parameter axis, an effect caused by irregular data sampling are clearly seen. Figures 1B and

1C portray the least-squares inverted CIG after 4 and 11 iterations, respectively. Figure 1D shows the result of pre-conditioned RLSM after 4 realizations. The image quality of Figure 1D is quite similar to that of Figure 1C. This confirms previous research in pre-conditioning strategies for least-squares migration algorithm (Prucha and Biondi (2001).

The structural image is computed by stacking CIGs along the ray parameter axis. The structural image obtained via migration is showed in Figure 2A. The structural images obtained via RLSM are displayed in Figure 2B (11 CG iterations) and 2C (4 CG iterations with preconditioning). Both least-squares methods lead to a better continuity of reflectors in the areas of low fold. Besides, an appreciable improvement in vertical resolution is also observed. The latter can be explained as follows. First, by imposing smoothness to the inverted CIG, we improve the coherency of the angle traces prior to stacking. In particular, part of the smearing produced by aperture limitation (non-flatness at high ray parameters) are attenuated and, therefore, the stacked common image gather can preserve high frequencies. In addition, the least-squares migration also functions as a de-blurring operator. The implicit deconvolution effect can be explained as follows. The modeling operator can be decomposed in two operators, a full band modeling operator \mathbf{L}_f followed by a band-limiting operator \mathbf{B} . In general, \mathbf{B} represents the fact that downward/upward continuation is carried out on a band-limited temporal frequency axis. During the inversion of the chained operator $\mathbf{B}\mathbf{L}_f$ we simultaneously try to invert the modeling operator and de-blur the operator \mathbf{B} . This is an important concept that could lead to high resolution migration algorithms where the migrated image can have a lateral and vertical resolution beyond the resolution limits imposed by data aperture and band-width. In particular, the addition of sparseness constraints to further increase vertical resolution is an aspect of current research.

In order to evaluate the accuracy of our algorithm, we compare an inverted CIG with a synthetic CIG obtained from bore-hole data. P-wave sonic and density logs in the area of the survey were used to compute zero offset synthetics to correlate the migrated image to the main geological targets in the area.

The red box in Figure 3 encloses the depth and ray parameter range that were used in our tests. After calibrating p-wave sonic velocities and densities to the seismic data, we proceed to compute shear wave velocities (not provided) using empirical expressions. The shear wave velocities are estimated by Castagna's (1985) mud-rock line formula $V_s = (V_p - 1360)/1.16 [m/s]$. This V_p/V_s relationship is valid for the background trend of clastic silicate rocks. The use of this approximation is reasonable in our case since most strata above our target interface consist of sandstone and/or mudstone.

The local V_p , density and estimated V_s traces were used to calculate angle dependent reflectivity using Aki & Richards' approximation (1980). The angle dependent

High resolution 3-D AVA Imaging

synthetic reflectivity is converted to time and convolved with a wavelet estimated from the data. This result is compared to the inverted CIG after depth-to-time conversion. Synthetic and inverted angle dependent reflectivities are provided in Figure 4. In general, the two angle gathers exhibit a high correlation at the target reflection (0.7s). We extract the AVA signature for the prominent event at time 0.7s (1500m in the original AVP gather). This event is associated to a high velocity contrast between the Ellerslie formation (marine sandstone) and the top of the Banff formation (siliclastics). The extracted AVA curves are shown in Figure 5. We can see that the inverted AVA reproduces quite well the synthetic AVA for angles in the 13 to 27 degrees range. It is clear, that the inversion does not provide reliable information at badly sampled angles (areas of deficient angular illumination).

Conclusions

The field data test shows that least-squares AVA migration can provide reliable amplitude information from sparse 3-D land data sets. Our algorithm can be used for deriving high resolution artifact-free CIGs that can be subsequently used to extract rock and/or fluid properties. It provides high quality common image gathers in the angle domain and, in addition, a migrated image that can be used to reconstruct the seismic volume (de-migrate).

Field data tests were used to confirm the validity of previous work on RLSM using well controlled simulations. We also observed that it is quite difficult to retrieve accurate amplitude estimates at small angles, which is probably caused by poor distribution of near-offset traces, and synthetic data confirmed this assumption. We are considering a simple parametrization of the CIG (via intercept amplitude and gradient) to constraint the behavior of the amplitude variations at small angles.

Acknowledgments

The Signal Analysis and Imaging Group at the University of Alberta would like to acknowledge financial support from the following companies: GeoX Ltd., EnCana Ltd., Veritas Geo-Services and the Schlumberger Foundation. This research has also been supported by The National Sciences and Engineering Research Council of Canada and the Alberta Department of Energy. We thank Brian Russel, Dean Rokosh, Uli Theune and Harold Huebscher for providing the WCSB data and assisting with the geology of the area.

References

Aki, K. and Richards, P. G., 1980. Quantitative seismology: W.H. Freeman & Co.
Biondi, B., and Palacharla, G. 1996, 3-D pre-stack migration of common-azimuth data: *Geophysics*, **61**, 1822-1832.

Castagna, J. P., Batzle, M. L., and Eastwood, R. L., 1985, Relationship between compressional wave and shear wave velocities in clastic silicate rocks: *Geophysics*, **50**, 571-581.
Fomel, S., and Claerbout, J. F., 2003, Multidimensional recursive filter preconditioning in geophysical estimation problems: *Geophysics*, **68**, 577-588..
Kuehl H. and Sacchi M.D., 2003, Least-squares wave-equation migration for AVP/AVA inversion: *Geophysics*, **68**, 262-273.
Prucha, M., Biondi, B., and Symes, W., 1999, Angle-domain common image gathers by wave-equation migration: 69th Ann. Internat. Mtg., Soc. Expl. Geophys., Expanded Abstracts, 824-827.
Prucha, M., Biondi, B., 2002, Subsalt event regularization with steering filters: 72nd Ann. Internat. Mtg., Soc. Expl. Geophys., Expanded Abstracts, 1176-1179.
Saad, Y., 1991, Numerical methods for large eigenvalue problems: URL <http://www-users.cs.umn.edu/saad/books.html>
Sava, P., Biondi, B., and Fomel, S., 2001, Amplitude-preserved common image gathers by wave-equation migration: 71st Ann. Internat. Mtg., Soc. Expl. Geophys., Expanded Abstracts, 296-299.
Trad, D., Ulrych, T. and Sacchi, M. D., 2003, Latest views of the sparse Radon transform: *Geophysics*: **68**, 386-399.
Wang, J., Kuehl, H. and Sacchi, M. D., 2003, Least-squares wave-equation AVP imaging of 3D common azimuth data: 73rd Ann. Internat. Mtg., Soc. Expl. Geophys., Expanded Abstracts, CDROM, 4 pages.
Xu, S., Chauris, H., Lambare, G., and Noble, M. S., 1998, Common angle image gather: a new strategy for imaging complex media: 68 th Ann. Internat. Mtg., Soc. Expl. Geophys., Expanded Abstracts, 1538-1541.

High resolution 3-D AVA Imaging

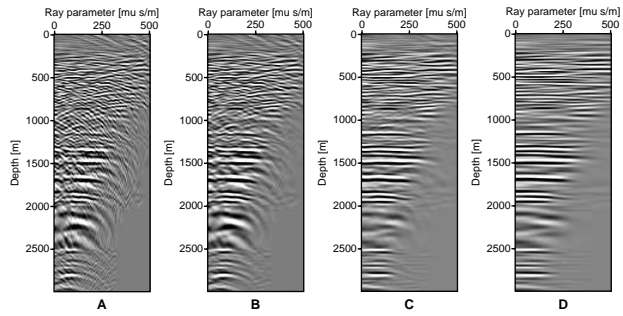


Fig. 1: Common image gathers for cross-line #10, in-line #71. A) CIG computed using AVA imaging (adjoint). B) CIG after 4 CG iterations of least-squares AVA imaging,. C) CIG after 11 CG iterations of least-squares AVA imaging, D) CIG after 4 PCG iterations of preconditioned least-squares AVA imaging,

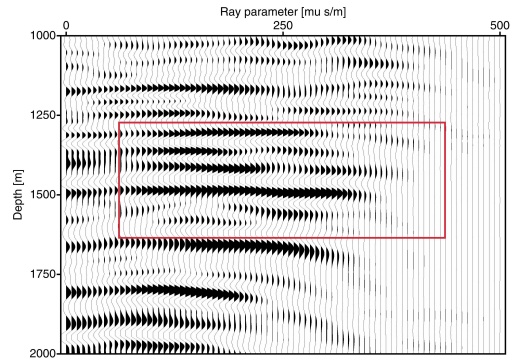


Fig. 3: Common image gather (AVP CIG) for midpoint in-line #76, cross-line #24. The box is converted to time and displayed in Figure 4B.

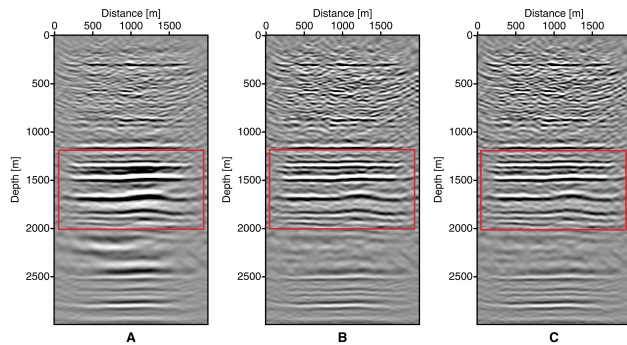


Fig. 2: Stacked image for in-line #71. A) Structural image computed by stacking migrated AVA gathers. B) Structural image computed by stacking AVA gathers obtained via least-squares AVA migration (11 iterations). C) Structural image computed by stacking AVA gathers obtained via preconditioned least-squares AVA migration (4 iterations).

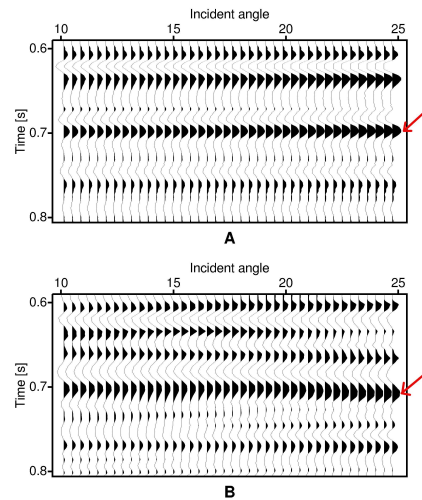


Fig. 4: Comparison between the synthetic CIG and the inverted CIG. A) Synthetic AVA CIG. B) Inverted AVA CIG. Both CIGs are displayed in time. The red arrows indicate the event of interest at depth 1500m. AVA curves for this event are shown in Figure 5.

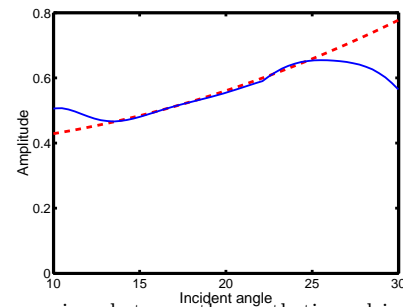


Fig. 5: Comparison between the synthetic and inverted AVA gathers. Red: synthetic. Blue: inverted.